processes

MDPI

Article

Catalytic-Level Identification of Prepared Pt/HY, Pt-Zn/HY, and Pt-Rh/HY Nanocatalysts on the Reforming Reactions of N-Heptane

Ramzy S. Hamied [1], Khalid A. Sukkar [2,*], Hasan Shakir Majdi [3], Zainb Y. Shnain [2], Mohammed Shorbaz Graish [2] and Luma H. Mahmood [2]

[1] Petroleum Technology Department, University of Technology-Iraq, Al-Sanna St., Baghdad 19006, Iraq
[2] Department of Chemical Engineering, University of Technology-Iraq, Al-Sanna St., Baghdad 19006, Iraq
[3] Chemical and Petroleum Industries Engineering Department, Al-Mustaqbal University College, Babylon 51015, Iraq
* Correspondence: khalid.a.sukkar@uotechnology.edu.iq

Abstract: The operation of reforming catalysts in a fixed bed reactor undergoes a high level of interaction between the operating parameters and the reaction mechanism. Understanding such an interaction reduces the catalyst deactivation rate. In the present work, three kinds of nanocatalysts (i.e., Pt/HY, Pt-Zn/HY, and Pt-Rh/HY) were synthesized. The catalysts' performances were evaluated for n-heptane reactions in the fixed bed reactor. The operating conditions applied were the following: 1 bar pressure, WHSV of 4, hydrogen/n-heptane ratio of 4, and the reaction temperatures of 425, 450, 475, 500, and 525 °C. The optimal reaction temperature for all three types of nanocatalysts to produce high-quality isomers and aromatic hydrocarbons was 500 °C. Accordingly, the nanocatalyst Pt-Zn/HY provided the highest catalytic selectivity for the desired hydrocarbons. Moreover, the Pt-Zn/HY-nanocatalyst showed more resistance against catalyst deactivation in comparison with the other two types of nanocatalysts (Pt/HY and Pt-Rh/HY). This work offers more understanding for the application of nanocatalysts in the reforming process in petroleum refineries with high performance and economic feasibility.

Keywords: fixed bed reactor; catalytic reforming; reaction temperature; bimetallic catalyst performance

Citation: Hamied, R.S.; Sukkar, K.A.; Majdi, H.S.; Shnain, Z.Y.; Graish, M.S.; Mahmood, L.H. Catalytic-Level Identification of Prepared Pt/HY, Pt-Zn/HY, and Pt-Rh/HY Nanocatalysts on the Reforming Reactions of N-Heptane. *Processes* **2023**, *11*, 270. https://doi.org/10.3390/pr11010270

Academic Editor: Blaž Likozar

Received: 23 December 2022
Revised: 7 January 2023
Accepted: 9 January 2023
Published: 14 January 2023

1. Introduction

The catalyst deactivation process is the main problem in catalytic reforming units [1]. Among the three general types of catalyst deactivation modes (i.e., coke formation, sintering, and poisoning), coke formation is the chief deactivation type in the reforming process [2–4]. All commercial catalysts in reforming units are significantly sensitive to coke formation problems due to the nature of reforming chemical reactions [5–8]. Therefore, many studies have worked to improve the catalyst resistance against deactivation using various additives as reaction promotors. Nanocatalysts are a modified category of catalysts that have a high available reaction surface area as well as unique structural specifications [9,10].

The quality of heavy naphtha can be enhanced if saturated normal hydrocarbons of a low octane rating are converted to their aromatic and isomer compounds [11–14]. The poor efficiency of traditional catalysts in the reforming process requires the production of new high-performance catalysts. Nanocatalysts are a new category of catalysts in which noble metals work on the initiation and promotion of active sites for the catalyst and provide high resistance against deactivation [10,15]. Often, nanocatalysts figure prominently in research activities due to their ability to control the reaction mechanism and the high yield of the desired products. Actually, the main requirements for catalysts in catalytic reforming reactions are to exhibit high efficiency for the aromatization and isomerization reactions of n-paraffin [16–22]. Thus, the modification of classical catalysts or nanocatalysts

by the incorporation of metals other than platinum will greatly affect reforming reactions. Lin et al. [23], Dong et al. [24], and Králik et al. [25] showed that the favorable activity, selectivity, and lifetime of catalysts are deeply dependent on the catalyst's composition, total surface area, crystalline structure, type of promotor, and metal dispersion.

From an industrial point of view, catalytic reforming contains different kinds of chemical reactions, like the dehydrocyclization reactions of normal-paraffins, isomerization reactions of normal-paraffins and naphthenes, cracking reactions, dealkylation reactions, and dehydrogenation reactions [26–30]. All of these reactions are considerably affected by the nature of the applied catalyst and feedstock specifications. Accordingly, to achieve these reactions successfully over nanocatalysts, the influence of each performance variable (e.g., activity, selectivity, and stability) must be evaluated [31–34]. Xu et al. [35] synthesized a Pt/KL zeolite nanocatalyst using the atomic layer deposition method. The authors found that the prepared nanocatalyst provided high activity in the n-heptane catalytic reforming reaction. It was noted that the toluene selectivity recorded a value of 67.3% with low methane gas. Keshavarz and Salabat [36] synthesized mono- and bimetallic Pt–Re/Al_2O_3 nanocatalysts for n-heptane reforming using different surfactants. The authors indicated that the nanocatalysts' activity significantly depended on the catalyst synthesis process. Kianpoor et al. [37] evaluated the activity of a prepared Au–Pt bimetallic nanocatalyst using purified naphtha as a feedstock for a reforming reaction. The operating conditions were a temperature of 485 °C, a weight hour space velocity (WHSV) between 2–6 h^{-1}, and an operating pressure of 5 bar. They found that the addition of Au to Pt in a ratio of 1:99 provided high naphthene conversion, high aromatics production, and low production of benzene and cracking gases. Sukkar [38] evaluated the catalytic reforming of n-heptane using prepared Pt/HY, Pt-Ge/HY, and Pt-Re/HY nanocatalysts. The author found that the addition of germanium as a promotor provided the highest catalyst performance in comparison with other types of nanocatalysts at an operating temperature of 480 °C. Yan et al. [39] improved the reforming of n-octane using a synthesized Pt/KY catalyst. They observed that the n-octane aromatization reaction provides a selectivity of 78.9%. Furthermore, the authors noted that the addition of potassium reduces the undesired products in the reforming process.

Designing and synthesizing an economically viable nanocatalyst that maintains high catalytic efficiency and stability is the most critical factor for the catalytic reforming of n-paraffin. Several improvements have been reported in the literature to prevent catalyst deactivation by coke formation [40–44] Most studies report enhancing the acidity of the catalyst and/or the use of noble metal promoters. Nevertheless, when designing nanocatalysts, the choice of a suitable metal promoter is becoming more challenging due to the complexity of catalytic reforming reactions [45–50]. According to a literature survey, nanocatalysts have not been employed at industrial scale until recently due to some practical limitations; additionally, deep studies at the pilot plant scale are required. Moreover, nanocatalysts are usually synthesized at a high cost in comparison with classical commercial catalysts [38,46]. The development of nanocatalysts needs effective criteria to evaluate their performance, cost, and lifetime. Therefore, the main aim of the present work is to synthesize efficient bimetallic nanocatalysts of Pt-Zn/HY and Pt- Rh/HY for the heptane catalytic reforming process. Additionally, this study evaluates the influence of the operating conditions on the performance of the catalytic reforming process to produce high-octane gasoline.

2. Materials and Methods

2.1. Materials

High-purity normal heptane (99.8%) purchased from Sigma-Aldrich (USA) was used in the present investigation as a feedstock for the reaction. Other chemicals used in the present study include hexachloroplatinic acid (H_2PtC_{l6}) of 40% wt. Pt, obtained from Honeywell Riedel-de-Haën™ (Germany), as well as sodium aluminate material ($NaAlO_2$) of 98.45% purity and sodium silicate material (Na_2SiO_3) of 98.27% purity from Fluka Corporation (Germany). Moreover, zinc chloride ($ZnCl_2$) of 99.31% purity and rhodium

chloride ($RhCl_3 \cdot nH_2O$) of 40% Rh purity from Shanxi-Kaida Company (China) were used in this study. Moreover, H_2 gas was used in a chemical reaction, with a purity of 99.98%, from Al-Mansour factory (Baghdad).

2.2. Synthesis of Nano Y-Zeolite

In the present work, nano-size Y-zeolite was prepared using the sol–gel technique. As a first step, an NaOH solution and $NaAlO_2$ were mixed together as a seed–gel mixture. Next, an Na_2SiO_3 solution was prepared in a 500-mL conical flask under stirring conditions for 30 min and aged at 25 °C for 30 h. Then, the first mixture was added to the second solution and stirred for 30 min at a mixing speed of 1600 rpm [33,38]. Next, a semisolid product was produced in an electrical furnace at an operating temperature of 100 °C for 24 h. This product was passed through a Buchner funnel to remove the aqueous phase. Then, the product was washed with deionized water four times. The final product of the prepared nano-Y-zeolite was subjected to a drying process to remove any physical water at 110 °C for 24 h. The produced Y-zeolite was then thermally treated by a calcination process using a muffle furnace in an oxygen environment at 550 °C for 5 h.

2.3. Preparation of Pt/HY, Pt-Zn/HY, and Pt-Rh/HY Nanocatalysts

Three kinds of reforming reaction nanocatalysts were prepared (i.e., Pt/HY, Pt-Zn/HY, and Pt-Rh/HY). The synthesized NaY zeolite was subjected to an ion-exchanging process using 3 N of an NH_4Cl solution. In this process, HY zeolite was synthesized after many stages of treatment [14,30]. Moreover, a modified impregnation method was applied using a sonication bath to synthesize the Pt/HY (0.3 Pt.%) nanocatalyst. Using this method, the HY zeolite was impregnated with a solution of H_2PtCl_6 via a dropwise approach under continuous mixing for 5 h at room temperature. The mixture was evaporated under continuous mixing conditions in the sonication bath for 6 h at 110 °C. The product was then subjected to drying process overnight at 110 °C. Furthermore, the produced nanocatalyst was calcined with oxygen at 550 °C for 5 h. The final step of the Pt/HY nanocatalyst synthesis included reduction by hydrogen at 400 °C for 5 h. Figure 1 summarizes the synthesis stages of the Pt/HY nanocatalyst.

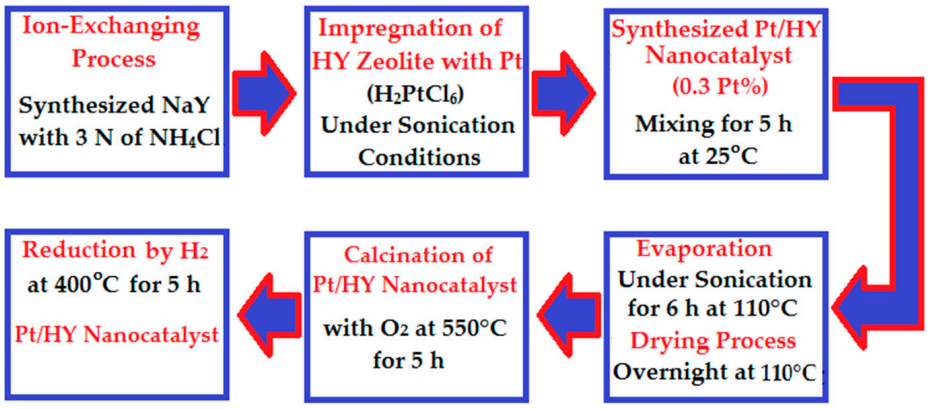

Figure 1. Main stages of the Pt/HY nanocatalyst preparation.

The preparation of bimetallic nanocatalysts requires the accurate weight of metal additions to ensure the needed percentages of each metal load. Accordingly, the synthesized Pt/HY nanocatalyst was used as a base catalyst for the other two types of bimetallic nanocatalysts. Then, Pt-Zn/HY and Pt-Rh/HY nanocatalysts were prepared by employing the co-impregnation method by adding each metal salt to the base nanocatalyst. Then, 1.2 mg/mL of zinc chloride salt solution was used in the synthesis of the Pt-Zn/HY nanocatalyst. A salt solution weighing 0.92 mg/L was added to the base nanocatalyst. However, the Pt-Rh/HY nanocatalyst was synthesized by immersion of each 10 g of Pt/HY nanocatalyst in 200 mL (0.3 wt%) of aqueous solution of RhCl3. The Pt-Zn/HY and Pt-

Rh/HY nanocatalysts were dried at 110 °C for 24 h, followed by a calcination step with oxygen at 500 °C for 5 h. The final step included the nanocatalyst reduction by H_2 at 450 °C for 3 h. Furthermore, to ensure the concentration of each metal on the catalyst at the required value, the chemical analysis results showed that the metal load on the catalyst support was 0.3, 0.32, and 0.31 for platinum, zinc, and rhodium, respectively. These values were checked with X-ray fluorescence (XRF) analysis. At this stage, the three kinds of prepared nanocatalysts (i.e., Pt/HY, Pt-Zn/HY, and Pt-Rh/HY) were ready for catalyst performance evaluation tests. Various types of nanocatalyst characterization devices were used, such as scanning electron microscopy (SEM, VEGA, Czech Republic), X-ray powder diffraction (XRD) (6000, Shimadzu, Japan), X-ray fluorescence (XRF) XRF (model type-7000, Shimadzu), and surface analysis using the Brunauer–Emmett–Teller (BET) of N_2 adsorption method.

2.4. Experimental System and Procedures

The performance of the prepared nanocatalysts was evaluated using a catalytic reforming unit with n-heptane as a feedstock. Figure 2 illustrates the schematic representation of the reaction rig. The reaction was carried out in a packed bed reactor constructed from stainless steel with a height and inner diameter of 25 and 2 cm, respectively. The reactor was enclosed by an electric furnace to provide the required reaction temperature at a constant heating rate. Additionally, a preheating system was supported before the reactor to provide an appropriate heating rate to the hydrocarbon mixture at a temperature of 140 °C. The inside reactor pressure was managed using sensitive pressure gauges. A calibrated flow meter was used to measure the volumetric flow rate of the hydrocarbon feedstock. Moreover, the reactor bulk temperature was controlled with the aid of a temperature control apparatus containing a temperature sensor (type K). An electrical furnace was utilized to supply the needed heating amount to the reactor at a constant distribution with constant operating temperature.

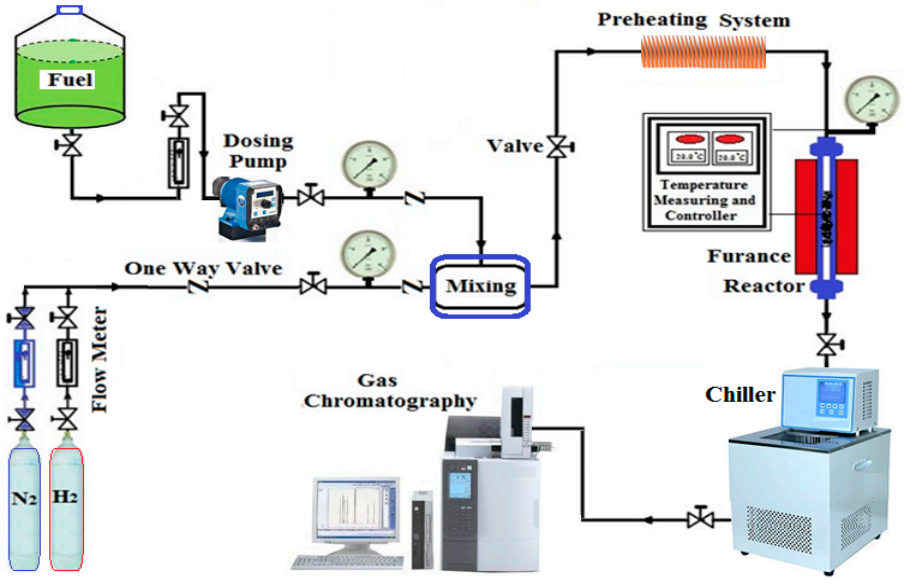

Figure 2. Schematic representation of the catalytic reforming rig.

Additionally, to assure the validity of the present work results, all sets of experiments were measured twice. Accordingly, an error analysis was estimated on the system variables (i.e., temperature, pressure, the flow rate of hydrogen gas, and the flow rate of n-heptane) by employing statistical analysis methods. Then, the uncertainty measurement was carried out in this system. Actually, the accuracy of the experimental results was estimated by calculating the standard errors of deviation (SD) between the measurements, which were recorded values of 0.01 to 1.4%. Moreover, all equipment and devices in the experimen-

tal apparatus were carefully calibrated to minimize experimental errors [24,47]. Table 1 illustrates the estimated experimental parameter uncertainties.

Table 1. Calculated experimental work uncertainties of catalytic reforming parameters.

Parameter	Uncertainty (%)
Total WHSV	±0.04
Temperature (°C)	±0.2
Pressure (bar)	±1.4
Hydrogen Flow Rate (cm^3/s)	±0.02
n-Heptane Flow Rate (cm^3/s)	±0.01

The performance of prepared Pt/HY, Pt-Zn/HY, and Pt-Rh/HY nano-catalysts was achieved in the catalytic process rig. For each kind of nanocatalyst, a mass of 10 g was loaded into the reaction zone inside the reactor. The catalyst was activated with H_2 gas before starting each experimental run at a temperature of 450 °C for 1 h. The catalytic reforming process was achieved at a pressure of 1 bar, WHSV of 4, hydrogen/n-heptane ratio of 4, and reaction temperatures of 425, 450, 475, 500, and 525 °C. Table 2 summarizes the main operating parameters of the reforming reaction of n-heptane. The reforming products were measured using a gas chromatography device (GC-2010, FID, Shimadzu, Japan), and nitrogen was used as a carrier gas in the analysis process. The capillary column type (ZB-FFAP) was applied with length of 30 m, I.D. of 0.32 mm, and FD = 0.50 µm. Moreover, the evaluation of catalyst selectivity regards the major task in determining the performance of the catalytic reforming process. Accordingly, the estimation of the prepared nanocatalysts' selectivity for the n-heptane reactions is the main criterion for the catalyst's efficiency as a function of operating temperature or reaction time. Actually, selectivity can be calculated as the ratio of the desired product to undesired product [6,34].

Table 2. Experimental operating conditions of the catalytic reforming process.

Operating Parameters	Value
Temperature range (°C)	425, 450, 475, 500, and 525
Pressure (bar)	1.0
Total WHSV	4.0
Hydrogen/n-Heptane ratio	4.0

3. Results and Discussion

3.1. Characterization of the Prepared Nano-Y-Zeolite

The structure of the prepared Y-zeolite was evaluated using XRD analysis, as presented in Figure 3, which shows that the prepared Y-zeolite had a high crystalline structure without impurities. The structural measurements showed that the SiO_2/Al_2O_3 ratio was 3. The resulting XRD pictures of the synthesized nano-Y-zeolite were in accordance with standard structural results [11,33,38]. Moreover, Table 3 summarizes the XRF results of the synthesized nano Y-zeolite composition. Additionally, it is clear such results are in accordance with XRD results. Furthermore, the morphological characteristics of the prepared Y-zeolite were measured using high-magnification SEM, as shown in Figure 4. The average particle size of the synthesized Y-zeolite was estimated using ImageJ software (version 1.8) [49]. Accordingly, by the analysis of the SEM image of the produced zeolite sample, the average particle size was determined accurately to be 48 nm. Furthermore, it was noted that the Y-zeolite has a spherical and uniform shape. Moreover, the zeolite's total surface area (SA) and pore volume (PV) were evaluated to be 610 m^2/g and 0.37 cm^3/g, respectively. Therefore, the high surface area was extremely effective in the n-heptane reforming process.

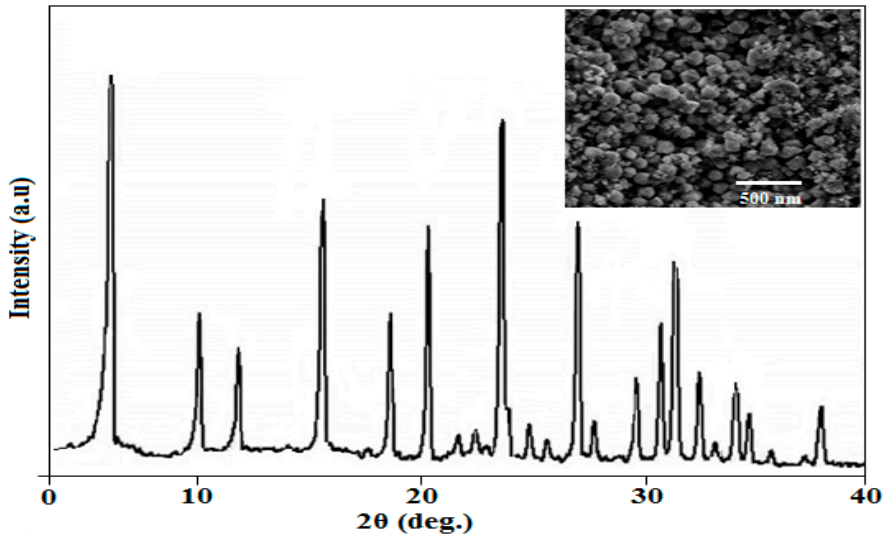

Figure 3. XRD and SEM results of the synthesized nano-size Y-zeolite.

Table 3. Chemical composition of the synthesized nano NaY-zeolite.

Compound	Weight%
SiO_2	56.47
Al_2O_3	19.08
Na_2O	24.10
CaO	0.210
MgO	0.083
Fe_2O_3	0.057
(Si/Al) ratio = 2.960	

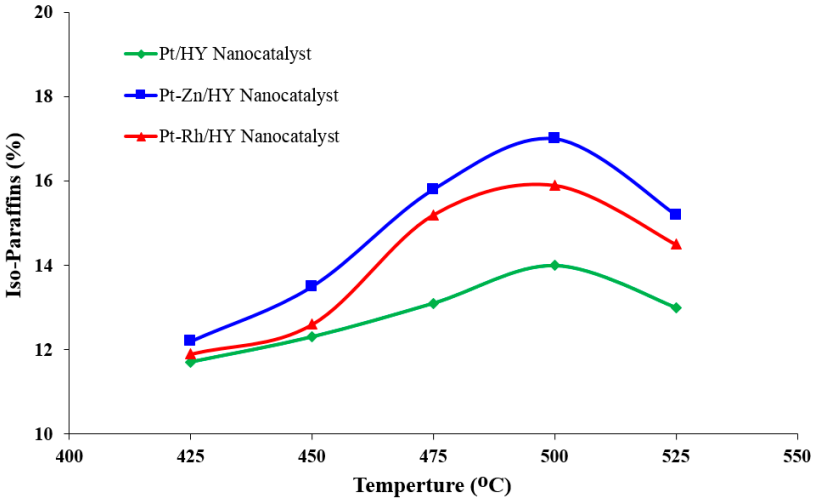

Figure 4. Influence of the catalytic reforming temperature on the iso-paraffin production rate over the synthesized Pt/HY, Pt-Zn/HY, and Pt-Rh/HY nanocatalysts.

3.2. Evaluation of the Nanocatalyst Surface Area

The catalyst's total surface area plays a key factor in determining the reaction mechanism to create the desired products. Table 4 shows the main properties of the synthesized nanocatalysts. The nanocatalysts (i.e., Pt/HY, Pt-Zn/HY, and Pt-Rh/HY) had surface areas of 612, 608, and 605 m^2/g, respectively, indicating that the catalysts' surface areas were reduced slightly due the presence of the second metal on the support surface to form a bimetallic nanocatalyst. Additionally, the results showed that the prepared nanocatalysts

had pore volumes of 0.42, 0.411, and 0.415 cm^3/g, respectively. Moreover, the nanocatalysts' pore volumes were generally constant, with only slight changes.

Table 4. Total surface area and pore volume of the prepared nanocatalysts.

Property	Pt/HY	Pt-Zn/HY	Pt-Rh/HY
Metal Load Wt. (%)	0.3 Pt	0.3% Pt and 0.31% Zn	0.3 % Pt and 0.32 % Rh
Surface Area (m^2/g)	608	584	593
Pore Volume (cm^3/g)	0.420	0.405	0.413

3.3. Evaluation of the Nanocatalysts' Activities

In catalytic reforming processes, the catalyst's performances (e.g., catalyst activity, selectivity, and lifetime) are key factors in determining the produced gasoline fuel quality. Figure 4 summarizes the number of generated iso-paraffins from the catalytic reforming process of n-heptane at different reforming temperatures. The results in Figure 5 show that the amount of iso-paraffin is deeply influenced by the operating temperature. The reaction temperature that provided the highest amount of iso-paraffins was 500 °C. Accordingly, at this operating temperature for the Pt-Zn/ HY-nanocatalyst, the iso-paraffin recorded values of 9.3, 13.9, 22.4, 23.5, and 20.1% at an operating temperature of 425, 450, 475, 500, and 525 °C, respectively. In addition, an increase in the operating reaction temperature above 500 °C had a significant effect on the number of isomers hydrocarbons, which is a positive indication of increasing branched hydrocarbons, which are associated with high-octane gasoline. Branched iso-paraffin products improve the quality of gasoline and increase the octane number dramatically [4,9,23,37]. Therefore, modern refineries focus on increasing the number of branched hydrocarbons and reducing the number of aromatics of hydrocarbons due to their pathogenic activity in relation to human health and the environment. Additionally, the introduction of Zn metal in the catalyst as a bimetal can promote the hydroisomerization activity by suppressing undesirable n-heptane reactions, such as hydrogenolysis.

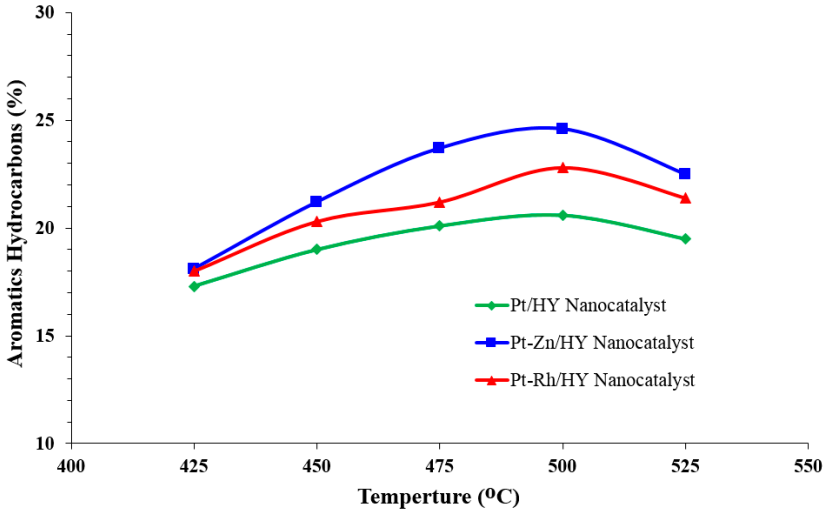

Figure 5. Influence of the catalytic reforming temperature on the aromatic hydrocarbon production rate over the synthesized Pt/HY, Pt-Zn/HY, and Pt-Rh/HY nanocatalysts.

In the catalytic reforming reactor, many mechanisms occur, depending on the catalyst activity and the reaction kinetics. A typical Pt/Al_2O_3 catalyst initiates the reforming mechanism by achieving hydrogenation and dehydrogenation reactions on the metal sites and hydroisomerization and aromatization reactions on the acid sites [10,16]. All of these reactions provide the final picture of the distribution of catalytic reforming products and

catalyst performance. The formation of aromatic hydrocarbons is a highly endothermic reaction. Then, operating under higher temperatures with low H_2 partial pressures in the reactor negatively impacts the catalyst's performance, causing coke to form on the catalyst's surface. Zhou et al. [19] and Bowker et al. [26] showed that the chemical reactions, such as hydroisomerization, cracking, and hydrogenolysis, are exothermic reactions and require lower operating temperatures with higher H_2 partial pressure.

Figure 4 illustrates the effect of the operating temperature on the distribution of iso-paraffins over the synthesized nanocatalysts. The reformate products consisted of a high percentage of branched isomers having high-octane gasoline. The results indicated that at an operating temperature of 500 °C, the formed isomers over the Pt/HY, Pt-Zn/HY, and Pt-Rh/HY nanocatalysts were 17.2, 15.7, and 13.8 mole%, respectively. The highest quantity isomers were formed over the Pt-Zn/HY catalyst. Moreover, the number of produced isomers decreased when the operating temperature rose above 500 °C due to cracking reactions. An increase in temperature over 500 °C will produce more gaseous products due to thermal cracking reactions [5,34].

Figure 5 shows the percentage of produced aromatic hydrocarbons (BTX) at different operating temperatures. The number of aromatics was highly influenced by the reaction temperature, with the highest number of aromatic hydrocarbons found at 500 °C for all three types of synthesized nanocatalysts. Therefore, as the reaction temperature increased in the reactor, the produced aromatics increased. Moreover, above 500 °C, the aromatic hydrocarbons underwent a clear reduction due to increased cracking reactions of n-heptane. Furthermore, the addition of other metals, such as Zn, in the nanocatalyst structure did not significantly affect the dehydrocyclization activity of n-heptane. Actually, Zn improved the reducibility of the Pt species by improving the Pt dispersion ability on the surface of the nanocatalyst. Hence, the bimetallic nanocatalysts (i.e., Zn and Rh) increased the number of acid sites on the catalyst. These metals also provided significant suppression of hydrogenolysis and cracking activities. The same observation was indicated by many authors, such as Arsentev et al. [10], Hanafi et al. [31], Keshavarz and Salabat [36].

From a thermodynamics point of view, Martínez et al. [4], Ahmedzeki et al. [8], and Shi et al. [45] showed that the maximum quantities of the desired reforming products, such as isomers and aromatics, are usually generated from chemical reactions at equilibrium conditions. Then, the operating pressure and temperature, in this case, can determine the equilibrium compositions of these compounds, and a perfect catalyst design can be achieved. Accordingly, the maximum number of desired hydrocarbons can be produced with minimal side reactions (cracking reactions). The present experimental results indicated that the chemical reactions of n-heptane are quite sensitive to the reaction temperature in the reactor. Therefore, researchers have sought the best operating temperature to enhance the production of high-octane gasoline [1,35]. Furthermore, Martínez et al. [4] noted that the presence of H_2 in the reforming reactor is beneficial in preventing catalyst deactivation and reducing undesirable by-product formation. Therefore, in the present investigation an H_2/H.Cs ratio with an acceptable value of 4 was applied. Actually, using high H_2/H.Cs ratios increased the energy cost. Thus, the lower boundary of H_2 can be dictated by the desired quantity for hydrocracking with low catalyst deactivation to save the energy consumed in the reforming system.

Figure 6 shows the effect of the operating temperature on the quality of the produced cracking gases. The three prepared nanocatalysts formed low-cracking products from n-heptane reforming, but the operating temperature played a key role in the distribution of cracking gases. At 500 °C, it was noted that the generated cracking gases for the synthesized Pt/HY, Pt-Rh/HY, and Pt-Zn/HY nanocatalysts recorded values of 15.3, 11.4, and 10.1 mole%, respectively. Accordingly, the present work was achieved at atmospheric pressure, which represents a severe condition that produced more gaseous products. However, the use of such operating conditions indicated that the Pt-Zn/HY nanocatalyst is the optimal catalyst, as it produced low-cracking products.

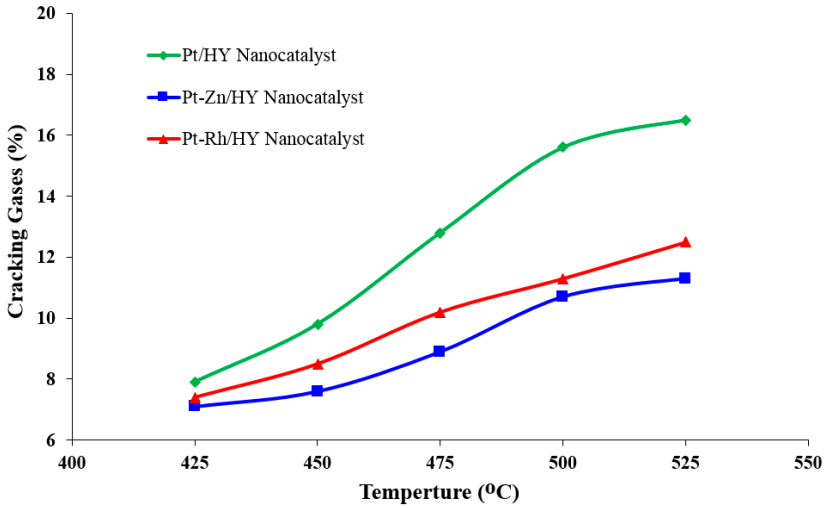

Figure 6. Influence of the catalytic reforming temperature on the cracking reaction over the synthesized Pt/HY, Pt-Zn/HY, and Pt-Rh/HY nanocatalysts.

Al-Shathr et al. [14], Zhang et al. [22], Said-Aizpuru et al. [29], and Rabe [46] indicated that the main variables that influence the activity of the applied catalyst in the catalytic reforming unit significantly depends on the operating temperature, hydrocarbon feed specifications, residence time, operating pressure, and H_2/HCs ratio. In the present work, it was noted that the reaction temperature is the chief factor that determines the quality of the produced reformate from the reaction. Moreover, the quality of the reformate from the reactions is also fundamentally dependent on the main reaction over the catalyst, such as hydroisomerization, aromatization, and cracking conversions. Then, from the perspective of management, the reaction temperature is the predominant factor that controls the product types in each reaction. Therefore, all prepared nanocatalysts (Pt/HY, Pt-Rh/HY, and Pt-Zn/HY) work to minimize the produced cracking gases (C_1-C_3) and seek a high rate of branched hydrocarbons, which are present in high-octane gasoline. In addition, in recent years, most petroleum refineries have focused on minimizing aromatics in the reformate due to environmental considerations [2,17,43].

On an industrial scale in a petroleum refinery, the catalytic reforming unit consists of three major reactors that differ in size. The first is the smallest, the second is larger, and the third is the largest. This difference in the reactor size is related to the nature of the chemical reactions that occur in each reactor. In the first one, high-speed reactions of hydrogenation/dehydrogenation are achieved. Furthermore, such reactions usually occur on the metal sites with endothermic behavior. Thus, a clear temperature drop is typically observed in this reactor. Moreover, slow reactions, such as isomerization and cyclization, are achieved in the second and third reactors [5,22].

3.4. Evaluation of n-Heptane Conversion

Figure 7 shows the results of the n-heptane total conversion at 500 °C over the Pt/HY, Pt-Zn/HY, and Pt-Rh/HY nanocatalysts at a WHSV of 4. At the initial reaction operation of 5 h, the total conversion gave values for each nanocatalyst of 72, 86.4, and 91.3%, respectively. The catalyst performance results with time indicated that the catalyst activity declined significantly due to carbon deposited on the active sites. Moreover, the bimetallic nanocatalysts showed higher stability in comparison with the monometallic nanocatalysts. The Pt-Zn/HY catalyst was highly stable and active in producing gasoline from n-heptane. The value of WHSV (4) provided the highest n-heptane conversion with a long lifetime, indicating it was highly stable. In catalytic reforming units, catalyst deactivation generally results from coke formation, poisoning, and sintering, with coking as the chief reason for deactivation [19,26,43]. Coke is formed due to some side reactions of naphthenic hydrocarbons [7].

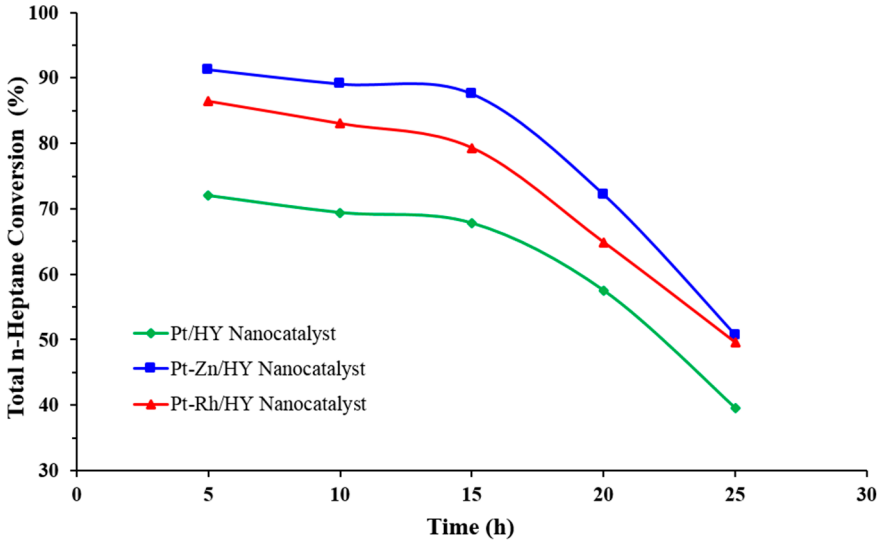

Figure 7. Relationship between the total reaction conversion of n-heptane into products of reformate with the reaction time at a temperature of 500 °C, WHSV = 4, and H_2/HCs = 4.

3.5. Evaluation of Catalyst Selectivity

The evaluation of the nanocatalysts' selectivity with reaction time allows for excellent control for the desired product distribution, including the production of iso-paraffins and aromatics. Figure 8 shows the variation in the catalyst selectivity of the three synthesized nanocatalysts with reaction time. The catalytic activity of the synthesized nanocatalysts was highly influenced by Zn loading with Pt, which produced a clear improvement in the selectivity toward the required products, with the Pt-Zn/HY nanocatalyst showing the highest value of selectivity of about 97.5%. This value was stable over time for more than 10 h and then gradually decreased until a value of 68.7 % was achieved at 25 h. Moreover, the other two nanocatalysts (i.e., Pt/HY and Pt-Rh/HY) gave selectivity values of 94.1% and 82.9%, respectively, at 5 h of reaction time.

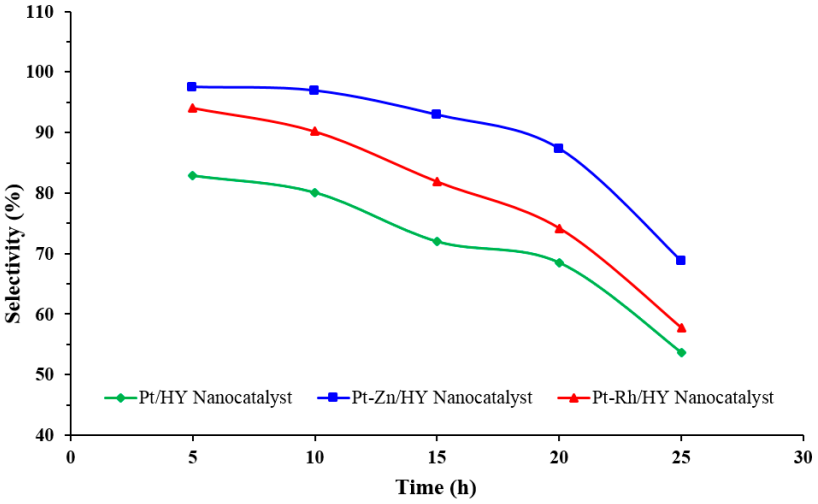

Figure 8. Selectivity of the synthesized nanocatalysts with reaction time at 500 °C, WHSV = 4, and H_2/HCs = 4.

The synthesized bimetallic Pt-Zn/HY nanocatalyst provided more stable operation characteristics for the catalytic reforming of n-heptane over the reaction time. This behavior was related to the influence of Zn, which is recognized for its effective stability with low amounts of cracking gases. On the other hand, the gradual decrease in the catalysts' selectivity is attributed to the low available nanocatalyst total surface reaction area due to

carbon deposition on the active sites. Moreover, the reduction in the total surface area will decrease the required number of available Lewis and Brønsted acid sites for the reaction mechanism [17,45]. Accordingly, the comprising of the present study results with the results of other authors, such as Keshavarz and Salabat [36] and Sukkar [38], and Singh et al. [42], it was observed that the prepared Pt-Zn/HY nanocatalyst showed high performance toward the n-heptane catalytic reforming reaction. Table 5 summarizes the comparison between the present work results with that of many authors over different catalyst types.

Table 5. The comparison of the present work results with the results of many authors over different kinds of catalysts (catalytic reforming of n-heptane).

Authors	Catalyst Type	Operating Temperture	Catalyst Selectivity%
Bowker et al. [26]	Pt–Sn/γ-Al_2O_3 Catalyst	400 °C	64.2 (Conv.)
Said-Aizpuru et al. [29]	Pt/γ-Al_2O_3-Cl Catalyst	410 °C	68.0
Xu et al. [35]	Pt/KL Zeolite Nanocatalyst	420 °C	84.3
Sukkar [38]	Pt-Ge/HY Nanocatalyst	480 °C	95.0
Shi et al. [45]	Pt/Beta Zeolite-Rb Catalyst	450 °C	78.2
Present Work	Pt-Zn/HY Nanocatalyst	500 °C	97.5

3.6. Reaction Mechanism over the Prepared Pt-Zn/HY Nanocatalysts

From a reaction mechanism point of view, HY-zeolite has many advantages, such as the high total surface area and larger-pore volume in comparison with classical reforming catalysts of Pt/Al_2O_3-Cl type [6,36,42]. In addition, HY-zeolite catalysts are characterized by their high ability to resist the continents that appeared in the feedstock. On the other hand, the main disadvantage of this type of catalyst is the high operating temperature in comparison with industrial reforming catalysts. Actually, Y-zeolite has a 3D structural network of hydrated aluminosilicate structures formed from the interlinked tetrahedral of SiO_4 and AlO_4 [30,50]. All these specifications make the Y-zeolite able to serve efficiently as a catalyst in different chemical reactions in the petroleum industry [13,25,39].

The use of n-heptane as a feedstock in the catalytic reforming process using the synthesized bimetallic nanocatalysts usually obeys the bifunctional mechanism [8,23]. The commercial catalysts Pt/Al_2O_3 and Pt-Re/Al_2O_3 are bifunctional in their reaction mechanism. As such, hydrogenation and dehydrogenation reactions occurred on the metal sites. In these reactions, the intermediate olefins usually form from the chemical reaction of creating paraffin. In contrast, aromatic hydrocarbons are formed from naphthene reactions. Furthermore, the isomerization and cracking reactions were achieved on the acid sites of the catalysts. Therefore, the n-heptane reaction included both kinds of active sites, and all reactions occurred in typical reforming catalysts. Figure 9 summarizes the main chemical reactions of the n-heptane conversion into products.

Additionally, benzene is produced from n-heptane on Pt sites. Moreover, the addition of Zn and Rh to the nanocatalysts provided a more stable catalyst with a significant conversion rate. Additionally, the results indicated higher selectivity in the direction of the desired products, including branched and aromatic hydrocarbons. Furthermore, in the present investigation, the prepared Pt-Zn/HY and Pt-Rh/HY nanocatalysts were more stable against catalyst deactivation problems. In addition, limited cracking gases were achieved under the best operating conditions. Accordingly, it can be seen that the addition of Zn to the nanocatalyst modified the acid sites dramatically, especially providing great resistance against coke formation. Therefore, a higher-than-normal production rate of the desired products will occur due to the high activity and suitable operating conditions in the reactor. All these parameters enhanced the nanocatalyst selectivity and stability over a long lifetime. The thermodynamics of catalytic reforming process provides the chief criteria for the evaluation of a catalyst's performance. The reaction of n-heptane over the Pt-Zn/HY nanocatalyst increased as the operating temperature rose to 500 °C, where the conversion was 91.4%; however, for further temperature increases, the n-heptane production clearly

decreased. Moreover, at 500 °C, the branched isomers and aromatics showed a selectivity of 97.5%. Figure 10 summarizes the catalytic reforming mechanism over the prepared Pt-Zn/HY nanocatalyst and presents the quality of the product distribution from the reforming of n-heptane. The main desired products were isomers and aromatics, while the undesirable products were cracking gases. Thus, the nanocatalyst can replace the classical industrial reforming catalysts with high performance, with a low deactivation rate and a low cost.

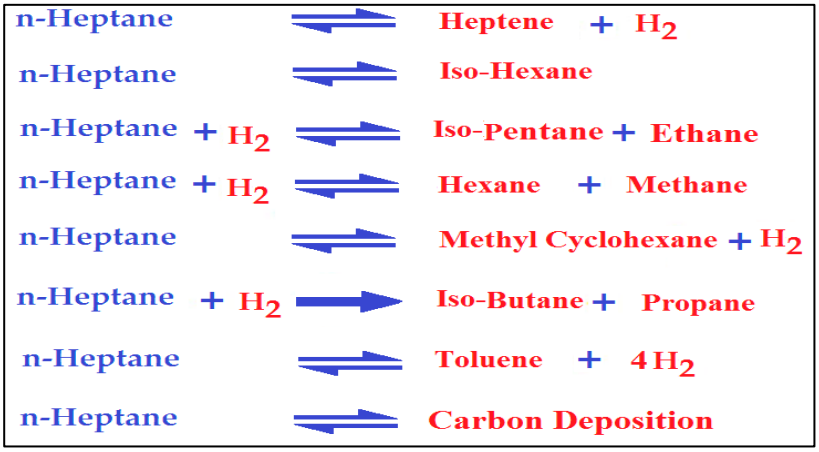

Figure 9. The suggested general reactions of the n-heptane catalytic reforming process.

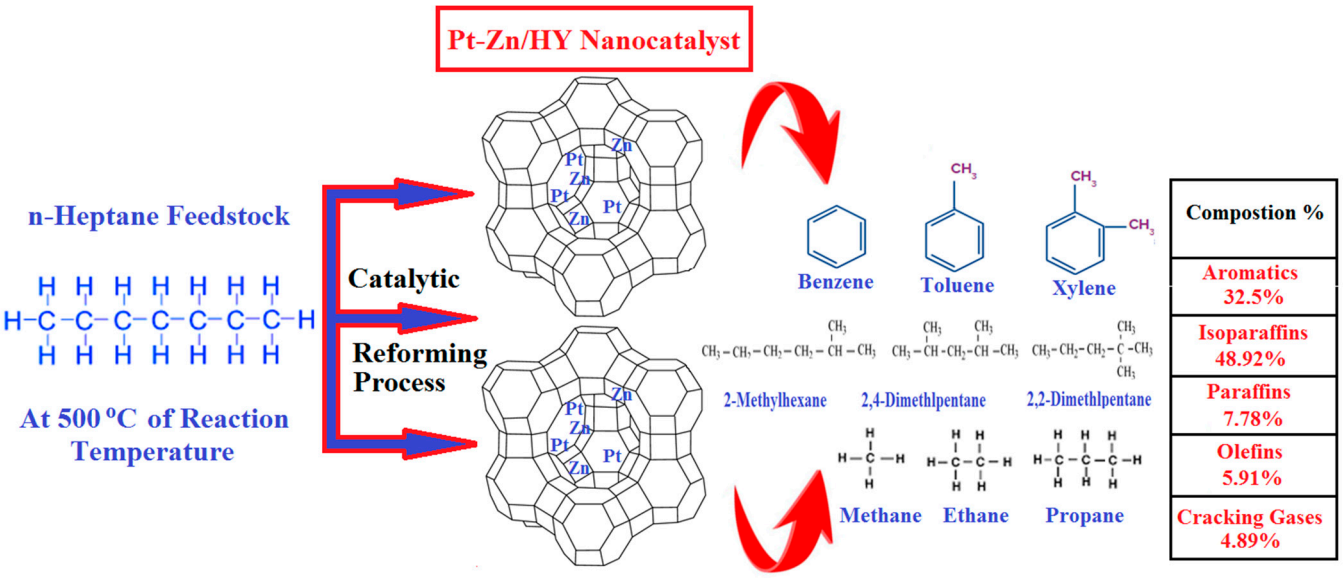

Figure 10. Schematic representation of the n-heptane reactions over the bimetallic Pt-Zn/HY nanocatalyst.

4. Conclusions

The three synthesized nanocatalysts (i.e., Pt/HY, Pt-Zn/HY, and Pt- Rh/HY) showed high performance toward n-heptane conversion in the catalytic reforming process. The results demonstrated that a temperature of 500 °C provided the highest product distribution of high-octane hydrocarbons, such as isomers and aromatics, with the greatest catalyst selectivity (97.5) for the Pt-Zn/HY nanocatalyst. Moreover, it was noted that at this operating temperature a low-value cracking gas (C1-C3) was obtained. The bimetallic catalysts Pt-Zn/HY and Pt- Rh/HY provided a high rate of activity toward the desired products with a low catalyst deactivation rate. Moreover, adding Zn and Rh to the nanocatalysts provided a more stable catalyst with a significant conversion rate. Additionally, the bimetallic nanocatalyst Pt-Zn/HY showed high stability against coke formation with a

long lifetime. This is attributed to the low reaction rate of unsaturated compounds that usually initiate deactivation by fouling. A gradual decrease in the catalyst selectivity was observed with time due to the low available catalyst total surface reaction area as a result of coke deposition on the active sites; this caused a clear reduction in the available Lewis and Brønsted acids. As a result, the synthesized nanocatalysts can replace the classical industrial reforming catalysts with an enhanced performance with a low cost.

Author Contributions: Conceptualization, K.A.S.; methodology, R.S.H.; formal analysis, K.A.S. and Z.Y.S.; investigation, K.A.S. and R.S.H.; data curation, R.S.H. and M.S.G.; writing—original draft preparation, R.S.H.; writing (review and editing), K.A.S.; visualization, L.H.M.; supervision, H.S.M.; project administration, H.S.M. and K.A.S. All authors have read and agreed to the published version of the manuscript.

Funding: This research received no external funding.

Institutional Review Board Statement: Not applicable.

Informed Consent Statement: Not applicable.

Data Availability Statement: Not applicable.

Acknowledgments: The authors are grateful to the Design & Production Research Unit at the Department of Chemical Engineering, University of Technology-Iraq and Al-Mustaqbal University College, Babylon, Iraq for their scientific support of this study.

Conflicts of Interest: The authors declare no conflict of interest.

References

1. Belopukhov, E.A.; Kir'yanov, D.I.; Smolikov, M.D.; Shkurenok, V.A.; Belyi, A.S.; Lavrenov, A.V.; Kleimenov, A.V.; Kondrashev, D.O. Investigation of fluorine-promoted Pt-Re/Al_2O_3 catalysts in reforming of n-heptane. *Catal. Today* **2021**, *378*, 113–118. [CrossRef]
2. Yang, Z.; Shi, Y.; Lin, Y.; Luo, L.; Song, N.; Lin, J.; Peng, C.; Sui, B.; Zhang, J.; Qian, G.; et al. Hierarchical pore construction of alumina microrod supports for Pt catalysts toward the enhanced performance of n-heptane reforming. *Chem. Eng. Sci.* **2022**, *252*, 117286. [CrossRef]
3. Yusuf, A.Z.; Aderemi, B.O.; Patel, R.; Mujtaba, I.M. Study of industrial naphtha catalytic reforming reactions via modelling and simulation. *Processes* **2019**, *7*, 192. [CrossRef]
4. Martínez, J.; Zúñiga-Hinojosa, M.A.; Ruiz-Martínez, R.S. A Thermodynamic Analysis of Naphtha Catalytic Reforming Reactions to Produce High-Octane Gasoline. *Processes* **2022**, *10*, 313. [CrossRef]
5. Shakor, Z.M.; AbdulRazak, A.A.; Sukkar, K.A. A detailed reaction kinetic model of heavy naphtha reforming. *Arab. J. Sci. Eng.* **2022**, *45*, 7361–7370. [CrossRef]
6. Saab, R.; Polychronopoulou, K.; Anjum, D.H.; Charisiou, N.D.; Goula, M.A.; Hinder, S.J.; Baker, M.A.; Schiffer, A. Effect of SiO_2/Al_2O_3 ratio in Ni/Zeolite-Y and Ni-W/Zeolite-Y catalysts on hydrocracking of heptane. *Mol. Catal.* **2022**, *528*, 112484. [CrossRef]
7. Argyle, M.D.; Bartholomew, C.H. Heterogeneous catalyst deactivation and regeneration: A review. *Catalysts* **2015**, *5*, 145–269. [CrossRef]
8. Ahmedzeki, N.S.; Al-Tabbakh, B.A.; Antwan, M.B.; Yilmaz, S. Heavy naphtha upgrading by catalytic reforming over novel bi-functional zeolite catalyst. *React. Kinet. Mech. Catal.* **2018**, *125*, 1127–1138. [CrossRef]
9. Tojo, C.; Buceta, D.; López-Quintela, M.A. On metal segregation of bimetallic nanocatalysts prepared by a one-pot method in microemulsions. *Catalysts* **2017**, *7*, 68. [CrossRef]
10. Arsentev, S.D.; Minasyan, V.T.; Grigoryan, S.L.; Tavadyan, L.A. Reforming of cyclohexane and n-heptane on nanosized Mo2C and W2C obtained by the carbidization of WO3 and MoO3 activated by vibrationally excited molecules of hydrogen. *React. Kinet. Mech. Catal.* **2017**, *120*, 219–230. [CrossRef]
11. Sun, Q.; Wang, N.; Yu, J. Advances in Catalytic Applications of Zeolite-Supported Metal Catalysts. *Adv. Mater.* **2021**, *33*, 2104442. [CrossRef]
12. Tregubenko, V.Y.; Belyi, A.S. Characterization of acid-modified alumina as a support for reforming catalysts. *Kinet. Catal.* **2020**, *61*, 130–136. [CrossRef]
13. Santa Cruz-Navarro, D.; Torres-Rodríguez, M.; Gutiérrez-Arzaluz, M.; Mugica-Álvarez, V.; Pergher, S.B. Comparative study of Cu/ZSM-5 catalysts synthesized by two ion-exchange methods. *Crystals* **2022**, *12*, 545. [CrossRef]
14. Al-Shathr, A.; Shakor, Z.M.; Majdi, H.S.; AbdulRazak, A.A.; Albayati, T.M. Comparison between artificial neural network and rigorous aathematical model in simulation of industrial heavy naphtha reforming process. *Catalysts* **2021**, *11*, 1034. [CrossRef]
15. Wang, J.; Zhu, P.; Liu, C.; Liu, H.; Zhang, W.; Zhang, X. Regulating encapsulation of small Pt nanoparticles inside silicalite-1 zeolite with the aid of sodium ions for enhancing n-hexane reforming. *Ind. Eng. Chem. Researc* **2022**, *61*, 9249–9261. [CrossRef]

16. Xu, D.; Wang, S.; Wu, B.; Zhang, B.; Qin, Y.; Huo, C.; Huang, L.; Wen, X.; Yang, Y.; Li, Y. Highly dispersed single-atom Pt and Pt clusters in the Fe-modified KL zeolite with enhanced selectivity for n-heptane aromatization. *ACS Appl. Mater. Interfaces* **2019**, *11*, 29858–29867. [CrossRef] [PubMed]
17. Sukkar, K.A.; Raouf, S.R.; Hamied, R.S. Investigation and simulation of catalytic reforming reactions of Iraqi heavy naphtha using Pt-Sn/Al_2O_3 and Pt-Ir/Al_2O_3 catalysts. *Eng. Technol. J.* **2013**, *33*, 2357–2380.
18. Epron, F.; Carnevillier, C.; Marécot, P. Catalytic properties in n-heptane reforming of Pt–Sn and Pt–Ir–Sn/Al_2O_3 catalysts prepared by surface redox reaction. *Appl. Catal. A Gen.* **2005**, *295*, 157–169. [CrossRef]
19. Zhou, J.; Zhao, J.; Zhang, J.; Zhang, T.; Ye, M.; Liu, Z. Regeneration of catalysts deactivated by coke deposition: A review. *Chin. J. Catal.* **2020**, *41*, 1048–1061. [CrossRef]
20. Almukhtar, R.; Hammoodi, S.I.; Majdi, H.S.; Sukkar, K.A. Managing Transport Processes in Thermal Cracking to Produce High-Quality Fuel from Extra-Heavy Waste Crude Oil Using a Semi-Batch Reactor. *Processes* **2022**, *10*, 2077. [CrossRef]
21. Demirbas, A.; Balubaid, M.A.; Basahel, A.M.; Ahmad, W.; Sheikh, M.H. Octane rating of gasoline and octane booster additives. *Petrol. Sci. Technol.* **2015**, *33*, 1190–1197. [CrossRef]
22. Zhang, P.; Yang, Y.; Li, Z.; Liu, B.; Hu, C. Preparation, characterization and naphtha aromatization performance of the catalytic reforming catalyst Pt/MY (M = Mg, Ba or Ce). *Catal. Today* **2020**, *353*, 146–152. [CrossRef]
23. Lin, C.; Pan, H.; Yang, Z.; Han, X.; Tian, P.; Li, P.; Xiao, Z.; Xu, J.; Han, Y.F. Effects of cerium doping on Pt–Sn/Al_2O_3 catalysts for n-heptane reforming. *Ind. Eng. Chem. Res.* **2020**, *59*, 6424–6434. [CrossRef]
24. Dong, X.J.; Shen, J.N.; Ma, Z.F.; He, Y.J. Robust optimal operation of continuous catalytic reforming process under feedstock uncertainty. *Int. J. Hydrog. Energy* **2022**, *47*, 35641–35654. [CrossRef]
25. Králik, M.; Gašparovičová, D.; Turáková, M.; Vallušová, Z.; Balko, J.; Major, P.; Kučera, M.; Puliš, P.; Milkovič, O. Hydrogenation of 4-chloronitrobenzenes over palladium and platinum catalysts supported on beta zeolite and γ-alumina. *Chem. Pap.* **2019**, *73*, 397–414. [CrossRef]
26. Bowker, M.; Aslam, T.; Roebuck, M.; Moser, M. The effect of coke lay-down on n-heptane reforming on Pt and Pt-Sn catalysts. *Appl. Catal. A Gen.* **2004**, *257*, 57–65. [CrossRef]
27. Sukkar, K.A.; Abd Al-Raheem, H.M.; Sabry, L.S.; Resym, L.A. New Development in Catalytic Reforming Process to Produce High Octane Gasoline. *J. Pet. Res. Stud.* **2014**, *5*, 223–244. [CrossRef]
28. Zainullin, R.Z.; Koledina, K.F.; Akhmetov, A.F.; Gubaidullin, I.M. Kinetics of the catalytic reforming of gasoline. *Kinet. Catal.* **2017**, *58*, 279–289. [CrossRef]
29. Said-Aizpuru, O.; Batista, A.T.; Bouchy, C.; Petrazzuoli, V.; Allain, F.; Diehl, F.; Farrusseng, D.; Morfin, F.; Joly, J.F.; Dandeu, A. Non monotonous product distribution dependence on Pt/γ-Al_2O_3-Cl catalysts formulation in n-heptane reforming. *Chem. Cat. Chem.* **2020**, *12*, 2262–2270.
30. Viswanadham, N.; Saxena, S.K.; Panwar, R.; Ray, A. A single-step catalytic process for the production of high-octane molecules from normal paraffins using zeolite supported bi-functional catalysts. *Chem. Eng. Process.-Process Intensif.* **2022**, *177*, 108990. [CrossRef]
31. Hanafi, S.A.; Gobara, H.M.; Elmelawy, M.S.; Abo-El-Enein, S.A.; Alkahlawy, A.A. Catalytic performance of dealuminated H–Y zeolite supported bimetallic nanocatalysts in Hydroizomerization of n-hexane and n-heptane. *Egypt. J. Pet.* **2014**, *23*, 119–133. [CrossRef]
32. Cerón, K.M.; Arias-Madrid, D.; Gallego, J.; Medina, O.E.; Chinchilla, L.E.; Cortés, F.B.; Franco, C.A. Catalytic Decomposition of n-C7 asphaltenes using tungsten oxides–functionalized SiO_2 nanoparticles in steam/air atmospheres. *Processes* **2022**, *10*, 349. [CrossRef]
33. Liu, Y.; Li, Z.; Yu, Q.; Chen, Y.; Chai, Z.; Zhao, G.; Liu, S.; Cheong, W.C.; Pan, Y.; Zhang, Q.; et al. A general strategy for fabricating isolated single metal atomic site catalysts in Y zeolite. *J. Am. Chem. Soc.* **2019**, *141*, 9305–9311. [CrossRef]
34. Tregubenko, V.Y.; Vinichenko, N.V.; Talzi, V.P.; Belyi, A.S. Catalytic properties of the platinum catalyst supported on alumina modified by oxalic acid in n-heptane reforming. *Russ. Chem. Bull.* **2020**, *69*, 1719–1723. [CrossRef]
35. Xu, D.; Wu, B.; Ren, P.; Wang, S.; Huo, C.; Zhang, B.; Guo, W.; Huang, L.; Wen, X.; Qin, Y.; et al. Controllable deposition of Pt nanoparticles into a KL zeolite by atomic layer deposition for highly efficient reforming of n-heptane to aromatics. *Catal. Sci. Technol.* **2017**, *7*, 1342–1350. [CrossRef]
36. Keshavarz, A.; Salabat, A. An Efficient Strategy in Microemulsion Systems to Prepare Mono-and Bimetallic Platinum-Rhenium Reforming Nanocatalyst with Remarkable Catalytic Performance. *Chem. Sel.* **2019**, *4*, 6094–6100. [CrossRef]
37. Kianpoor, Z.; Falamaki, C.; Parvizi, M.R. Exceptional catalytic performance of Au–Pt/γ-Al_2O_3 in naphtha reforming at very low Au dosing levels. *React. Kinet. Mech. Catal.* **2019**, *128*, 427–441. [CrossRef]
38. Sukkar, K.A. Evaluation of transport processes in a catalytic reforming reactor with high performance nanocatalysts. *IOP Conf. Ser. Mater. Sci. Eng.* **2021**, *1067*, 012149. [CrossRef]
39. Yan, M.; Xu, D.; Wang, S.; Wu, B.; Yang, Y.; Li, Y. Selective regulation of Pt clusters inside KY zeolite using atomic layer deposition for n-octane reforming. *Fuel* **2022**, *330*, 125671. [CrossRef]
40. Daligaux, V.; Richard, R.; Manero, M.H. Deactivation and regeneration of zeolite catalysts used in pyrolysis of plastic wastes—A process and analytical review. *Catalysts* **2021**, *11*, 770. [CrossRef]
41. Lutz, W. Zeolite Y: Synthesis, modification, and properties—A case revisited. *Adv. Mater. Sci. Eng.* **2014**, *2014*, 724248. [CrossRef]

42. Singh, B.K.; Lee, S.; Na, K. An overview on metal-related catalysts: Metal oxides, nanoporous metals and supported metal nanoparticles on metal organic frameworks and zeolites. *Rare Met.* **2020**, *39*, 751–766. [CrossRef]
43. Ren, X.Y.; Cao, J.P.; Zhao, S.X.; Zhao, X.Y.; Feng, X.B.; Liu, T.L.; Li, Y.; Zhang, J.; Wei, X.Y. Insights into coke location of catalyst deactivation during in-situ catalytic reforming of lignite pyrolysis volatiles over cobalt-modified zeolites. *Appl. Catal. A Gen.* **2021**, *613*, 118018. [CrossRef]
44. Talaghat, M.R.; Karimi, M.S. Operation parameters effect on yield and octane number for monometallic, bimetallic and trimetallic catalysts in naphtha reforming process. *Energy Sources Part A Recovery Util. Environ. Eff.* **2020**, *42*, 176–193. [CrossRef]
45. Shi, Y.; Zhou, Q.; Qin, Z.; Wu, Z.; Jiao, W.; Dong, M.; Fan, W.; Wang, J. Promoting effect of alkali metal on the catalytic performance of hierarchical Pt/Beta in the aromatization of n-heptane. *Microporous Mesoporous Mater.* **2022**, *343*, 112189. [CrossRef]
46. Rabe, S.; Vogel, F.; Truong, T.B.; Shimazu, T.; Wakasugi, T.; Aoki, H.; Sobukawa, H. Catalytic reforming of gasoline to hydrogen: Kinetic investigation of deactivation processes. *Int. J. Hydrog. Energy* **2009**, *34*, 8023–8033. [CrossRef]
47. Zhang, H.; Zhao, W.; Jiang, A.; Huang, Q.Y.; Wang, H.; Ding, Q. Dynamic Simulation of Continuous Catalytic Reforming Process Based on Simultaneous Solution. *Processes* **2021**, *9*, 1347. [CrossRef]
48. Esmaeili, E.; Rashidi, A.M.; Khodadadi, A.A.; Mortazavi, Y.; Rashidzadeh, M. Palladium–Tin nanocatalysts in high concentration acetylene hydrogenation: A novel deactivation mechanism. *Fuel Process. Technol.* **2014**, *120*, 113–122. [CrossRef]
49. Crouzier, L.; Feltin, N.; Delvallée, A.; Pellegrino, F.; Maurino, V.; Cios, G.; Tokarski, T.; Salzmann, C.; Deumer, J.; Gollwitzer, C.; et al. Correlative analysis of the dimensional properties of bipyramidal titania nanoparticles by complementing electron microscopy with other methods. *Nanomaterials* **2021**, *11*, 3359. [CrossRef] [PubMed]
50. Tavares, F.; Mohamed, H.O.; Kulkarni, S.R.; Morlanés, N.; Castaño, P. Decreasing the coking and deactivation of a reforming Ni-Ce/Al_2O_3 catalyst with intraparticle SiC in hydrogen production routes. *Fuel* **2023**, *337*, 127058. [CrossRef]